Heliyon 10 (2024) e38577

Contents lists available at ScienceDirect

Heliyon

journal homepage: www.cell.com/heliyon

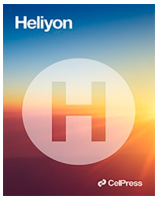

Research article

Fabrication of injectable, adhesive, self-healing, superabsorbent hydrogels based on quaternary ammonium chitosan and oxidized pullulan

Qian He [a], Xiaoyue Ding [b], Jun Deng [c], Yanze Zhang [b], Xiaoyi Wang [d], Dan Zhan [c], Oseweuba Valentine Okoro [e], Lizhao Yan [f,**], Armin Shavandi [e], Lei Nie [b,*]

[a] *Emergency Department, Wuhan No.7 Hospital, Wuchang District, 430061, Wuhan, China*
[b] *College of Life Sciences, Xinyang Normal University (XYNU), Xinyang, 464000, China*
[c] *Health Management and Physical Examination Department, Hubei Third People's Hospital, Jianghan University, Qiaokou district, 430030, Wuhan, China*
[d] *Department of Nutrition, Hubei Third People's Hospital, Jianghan University, Qiaokou district, 430030, Wuhan, China*
[e] *Université libre de Bruxelles (ULB), École polytechnique de Bruxelles - BioMatter unit, Avenue F.D. Roosevelt, 50 - CP 165/61, 1050, Brussels, Belgium*
[f] *Department of Hand Surgery, Union Hospital, Tongji Medical College, Huazhong University of Science and Technology, Wuhan, 430022, China*

ARTICLE INFO

Keywords:
Chitosan
Schiff base reaction
Hydrogel
Injectable
Cellular compatibility

ABSTRACT

Injectable hydrogels, which are polymeric materials that are characterized by their ability to be injected in a liquid form into cavities and subsequently undergo in situ solidification, have garnered significant attention. These materials are extensively used in a range of biomedical applications. This study synthesized several injectable composite hydrogels through the mild Schiff base reaction while imposing different concentrations of quaternary ammonium chitosan and oxidized pullulan. Subsequent characterizations revealed a consistent and coherent porous structure within the hydrogels with smooth inner walls. The hydrogels were also determined to possess good adhesion, mechanical properties, self-healing ability, and injectability. Furthermore, antimicrobial tests against *Escherichia coli* and *Staphylococcus aureus* demonstrated antibacterial properties, which improved with increasing concentrations of quaternary ammonium chitosan. Co-culturing with skin fibroblasts demonstrated that the injectable hydrogels exhibited favourable biocompatibility and the capacity to boost cellular activity, thus underscoring its potential for use in biomedical applications.

1. Introduction

Hydrogels, formed by physically or chemically crosslinking polymer chains, possess hydrophilic properties and 3-dimensional networks [1]. Due to their physicochemical characteristics similar to human tissues, hydrogels have become highly valuable materials in the medical field, especially in controlled drug delivery, regenerative medicine, biological adhesion, biosensing, and 3D cell culture techniques, among many other areas [2–5]. Hydrogels can be directly injected or transplanted into body tissues as functional

* Corresponding author.
** Corresponding author.
E-mail addresses: yanlizhaozzz@gmail.com (L. Yan), nieleifu@yahoo.com, nielei@xynu.edu.cn (L. Nie).

https://doi.org/10.1016/j.heliyon.2024.e38577
Received 1 August 2024; Received in revised form 26 September 2024; Accepted 26 September 2024
Available online 27 September 2024

materials to create sustained-release drug depots. This allows for higher drug concentrations at lesion sites, making them particularly suitable for targeted drug delivery systems [6].

Injectable hydrogels are distinctive biomaterials with rheological properties that allow them to flow under shear stress. This enables their passage through narrow syringes for administration, after which they regain their original mechanical properties *in vivo* [7–10]. Injectable hydrogels have garnered significant interest for their potential in the biomedical field. For example, the design of self-healing injectable hydrogels enhances their self-repair capability and stability after injection [11,12]. The mechanical strength of hydrogels typically inversely correlates with their injectability, making it challenging to develop hydrogels that possess both high mechanical strength and good shear-thinning injectability [13,14]. Previous studies have successfully prepared high-strength, injectable supramolecular hydrogels by constructing multiple hydrogen bond systems [10,15]. Injectable hydrogels can function as drug delivery carriers, offering sustained release of therapeutic agents directly at lesion sites, which enhances treatment effectiveness and minimizes side effects [16–18]. Some injectable hydrogels exhibit rapid and firm adhesion to various tissues, offering new possibilities for tissue repair and regeneration. Injectable hydrogels, when employed, can reduce the need for invasive surgery and enable personalized treatment based on individual patient conditions, demonstrating promise in the realm of personalized treatments. Research on injectable hydrogels is advancing, providing innovative therapeutic options and enhancing treatment outcomes and patient quality of life [19–21].

Currently, hydrogels can be produced using several materials, including synthetic polymers, natural polymers, and the incorporation of nanoparticles. For instance, Ding et al. utilized natural polysaccharide monomers as base materials and introduced varying amounts of chitosan to prepare a flexible composite hydrogel [22]. Seo et al. synthesized a conductive hydrogel with sensing and antibacterial functionalities using polyvinyl alcohol (PVA) and hyaluronic acid (HA) as raw materials [23]. Wu et al. used nano-clay and rare earth elements to prepare a composite luminescent hydrogel with good mechanical properties and acid-base sensitivity through copolymerization of acrylamide and 2-acrylamido-2-methylpropanesulfonic acid [24]. Marine biomaterials play a significant role in biomedical materials due to their abundant resources, wide distribution, and advantages such as diverse functionality, good malleability, and low toxicity [25–28]. Among them, chitin the second-largest natural polymer on earth after cellulose, is widely found in insects, crustacean shells, and fungal cell walls [29,30].

31. Chitosan (the deacetylated version of chitin) contains numerous free active functional groups in its molecular side chains, including amino, carboxyl, and hydroxyl groups [32]. These functional groups can act as modification sites, altering chitosan through physical, chemical, and biological methods to create hydrogel materials with improved biological performance. Researchers have improved the solubility of chitosan in water by introducing hydrophilic groups to its active sites through chemical reactions like alkylation [33], acylation [34], sulfonation [35], nitration [36], and halogenation [37]. These modifications enabled the successful preparation of chitosan derivatives with improved solubility in water, such as chitosan quaternary ammonium salts, carboxymethyl chitosan, N-carboxybutyl chitosan, and chitosan hydrochloride. Among them, chitosan quaternary ammonium salts not only inherit the advantages of chitosan itself but also exhibit greatly improved water solubility and antibacterial properties [38–44]. The multifunctional hydrogels could be fabricated via compositing chitosan quaternary ammonium with other polymers or nanoparticles [45]. Ma et al., have prepared QCMC-HA-PEG hydrogels based on quaternary ammonium-modifed carboxymetyl chitosan, hyaluronic acid, and 8-arms polyethylene glycol aldehyde for wound healing applications, the fabricated QCMC-HA-PEG hydrogels could accelerate the wound healing process via promoting skin epithelization, collagen deposition, and inflammatory regulation [46].

Pullulan is synthesized by microorganisms such as *Aureobasidium pullulans* through the biotransformation process of carbon sources such as sucrose or soluble starch [47–49]. It is a colorless, tasteless, and odorless biopolymer that is characterized by numerous hydrophilic groups, such as hydroxyl groups, in its molecular chain, making it highly soluble in water. Pullulan is insoluble in organic solvents such as ethanol, ether, acetone, and chloroform. Additionally, due to its high safety, heat resistance, salt resistance, acid-base resistance, and good plasticity, pullulan is widely used in various fields, including food additives, pharmaceutical manufacturing, daily chemicals, construction materials, and environmental protection [49–51]. Moreover, pullulan can react with sodium periodate to generate oxidized pullulan, which is an efficient crosslinking agent and can be used to crosslink with chitosan to prepare hydrogels with specific properties [52].

In this study, polymeric materials were prepared by attaching quaternary ammonium groups to the chitosan chain to produce quaternary ammonium chitosan, after which oxidation reactions were implemented to produce aldehyde-functionalized oxidized pullulan. The success of the grafting and oxidation reactions was assessed using infrared and nuclear magnetic resonance methods. Subsequently, two synthesized quaternary ammonium salt chitosan and oxidized pullulan were used to prepare hydrogel materials via Schiff base reaction. The hydrogels' microstructure, water absorption, swelling, rheological, adhesion, and antibacterial properties were characterized and tested. Additionally, culturing of the human fibroblast cells in the presence of hydrogel materials was undertaken to assess their compatibility and impact on cell activity.

2. Materials and methods

2.1. Materials

Chitosan (degree of deacetylation ≥95 %, viscosity 100–200 mPa s), pullulan, 2,3-epoxypropyl trimethylammonium chloride, sodium periodate, and methylene blue were sourced from Shanghai Macklin Biochemical Technology Co., Ltd. Cell Counting Kit-8 (CCK-8) assay kit, fetal bovine serum, phosphate buffered saline (PBS), streptomycin mix, and high-glucose culture medium were purchased from Beijing Solabao Co., Ltd. Nutrient Agar (NA) medium and Lysogeny Broth (LB) medium were bought from Qingdao High-tech Industrial Park Haibo Biotechnology Co., Ltd. All reagents were purchased and used directly without further purification.

2.2. Preparation of quaternary ammonium chitosan (QCS)

Quaternary ammonium chitosan was prepared in accordance with a method in the literature [53]. Briefly, 2.0 g of chitosan powder was added to 120 mL of deionized water at room temperature. The mixture was then stirred magnetically (120 rpm) for 10 min for complete dispersal. Subsequently, 15 mL of ice-cold acetic acid solution was added, and stirring was continued till it dissolved into a pale-yellow transparent solution. Next, 200 mg of 2,3-epoxypropyl trimethylammonium chloride powder was introduced to the solution, at 40 °C for 8 h, for reaction execution. At the end of the reaction, the product mixture was cooled to room temperature, and the solution was dialyzed for 3 days using deionized water. The dialysed solution was subsequently freeze-dried, and the dried QCS was obtained for later use.

2.3. Preparation of oxidized pullulan (OPL)

The preparation of oxidized pullulan polysaccharides follows previous research methods [54]. Briefly, 12.0 g of pullulan was introduced in deionized water (300 mL) and stirred continuously at 120 rpm for one day until fully dissolved. The beaker was wrapped with tin foil to ensure a dark environment (sodium periodate needs to be shielded from light), and then sodium periodate (10 g) was introduced to the pullulan solution with continuous stirring for 24 h to ensure complete reaction. The resulting solution was then dialyzed (molecular cutoff of the dialysis membrane was 3 kDa) for approximately 5 days. The dialyzed product was first cooled at 4 °C for 1 day and then freeze-dried for 3 days to obtain purified OPL.

2.4. The QCS/OPL hydrogel preparation

The preparation process of QCS/OPL hydrogel is based on previous research methods [55]. The QCS (0.25 g) was introduced to deionized water (5 mL) to obtain solution A, and OPL (0.25 g) was introduced to deionized water (5 mL) to obtain solution B. Both solutions were inserted in a 60 °C water bath and stirred for 24 h for complete dissolution. Both solutions A and B were mixed and reacted for about 1 min to obtain QCS/OPL hydrogels. According to weight ratios of solution A and solution B at 1:1, 4:1, and 9:1, QCS/OPL 11, QCS/OPL 41, and QCS/OPL 91 hydrogels were fabricated, respectively.

2.5. Assessment via Fourier Transform infrared (FT-IR) spectroscopy

FT-IR spectroscopy was utilized to verify the successful synthesis of QCS and OPL and the chemical interactions in hydrogels. An appropriate amount (0.5 g) of freeze-dried QCS, OPL, and hydrogel powders were mixed with re-crystallized KBr, ground into pellets, and dried at 50 °C to remove moisture completely. Then, FT-IR spectroscopy (FT-IR, Nicolelis50, Thermo Fisher Scientific) was employed to scan the samples in the range of 500–4000 cm^{-1}, and 64 times scan for each spectrum using a resolution of 1 cm^{-1}.

2.6. ^1H nuclear magnetic resonance (^1H NMR) spectroscopy assessment

^1H NMR spectroscopy was further proved to synthesize QCS and OPL successfully. An appropriate amount (0.05 g) of freeze-dried QCS and OPL was added to 0.5 mL of D_2O, respectively, dissolved completely at 37 °C, and then transferred to NMR tubes for ^1H NMR characterization using an NMR spectrometer (600 MHz, JEOL ECZ600R/S3).

2.7. Microscopic morphology characterization

The fabricated QCS/OPL 11, QCS/OPL 41, and QCS/OPL 91 hydrogel samples were introduced into liquid nitrogen to solidify and then fractured. Platinum sputtering was applied to the fractured surface (coating thickness: 10 nm). After that, SEM (Hitachi S-4800, Hitachi) was used for imaging under an accelerating voltage.

2.8. Water swelling performance

The water swelling measurement refers to previous research work [56]. The hydrogel (freeze-dried) sample (m_1 in g) was immersed in PBS with a pH of 7.4. At specified time intervals, the retrieval of the hydrogel was undertaken, with the surface water wiped off. The sample was then measured as m_2 (g). Until no further mass change was observed, the test was finished. The water absorption rate (*WAR*) of different hydrogel samples was then calculated as follows:

$$WAR = \frac{m_2 - m_1}{m_1} \times 100\% \quad (1)$$

where *WAR* represents the water absorption rate of the hydrogel, m_1 (g) represents the dry mass of the freeze-dried hydrogel sample before insertion into the PBS, and m_2 (g) represents the hydrogel sample mass after immersion in PBS at different time intervals. Five parallel tests were conducted on each sample, followed by calculating the mean and variance.

2.9. Rheological property test

The fully swollen samples were stored at 4 °C for 6 h to ensure that the hydrogels achieved a completely uniform gel state. The rheological characteristics of the hydrogel were assessed for time, temperature, and oscillation frequency using a rheometer (Discovery HR-20, Waters Corporation).

2.10. Antibacterial property test

Escherichia coli and *Staphylococcus aureus,* which are Gram-negative and Gram-positive bacteria, respectively, were selected as representatives for the antibacterial property analysis of QCS/OPL hydrogels [57]. Initially, the preserved bacterial strains were retrieved, activated, purified, and cultured on a large scale. Subsequently, LB liquid culture medium (10 mL) and freeze-dried hydrogel sample (0.1 g) were introduced to a test tube, followed by the bacterial solution (10 μL) with a concentration of 2×10^9 CFU/mL and the tube sealed with a stopper. As a negative control, LB liquid culture medium (10 mL) was introduced to a test tube, followed by the bacterial solution (10 μL) with a concentration of 2×10^9 CFU/mL and the tube was sealed with a stopper. The sealed test tube was then incubated on a shaker for 6 h at 37 °C. After incubation, the absorbance at the wavelength of 600 nm (OD_{600}) was measured using an ultraviolet–visible spectrophotometer.

2.11. Cell culture

The skin fibroblast cells (NIH/3T3 cells, CRL-1658™, ATCC) of a mouse were utilized to investigate QCS/OPL hydrogels cytocompatibilities [58]. Culturing of the NIH/3T3 cells occurred in a Dulbecco's Modified Eagle Medium (DMEM) that had been supplemented with 10 % fetal bovine serum (FBS) and 1 % penicillin-streptomycin. The cells were incubated at 37 °C in a 5 % CO_2 atmosphere. The cells were passaged using trypsinization, and those at passage 5 were utilized for the subsequent tests.

2.12. Cell Counting Kit-8 (CCK-8) assay

Prior to conducting cell experiments, QCS/OPL hydrogel samples were sterilized by immersing them in 75 v/v% ethanol for 6 h. After the ethanol treatment, the hydrogels were rinsed 5 times with a sterile PBS solution. Finally, the samples were subjected to ultraviolet light to complete the sterilization process, for 4 h. 100 μL of NIH/3T3 cells suspension was introduced to each well of a 96-well plate, which was pre-cultured in an incubator for 24 h. Then, the hydrogel extraction solution (100 μL) was introduced to the culture plate, then cultured in an incubator and additional 24 h. Next, CCK-8 solution (10 μL) was introduced to each well, and the plate was incubated for 4 h in the cell culture incubator. After incubation, the absorbance at the wavelength of 450 nm (OD_{450}) was measured using a microplate reader [59].

2.13. Scratch test

A clear cell isolation area was generated by culturing inserts to evaluate the migration ability of fibroblasts on different hydrogel scaffolds [60]. Firstly, 70 μL of NIH/3T3 cells suspension with a density of 4×10^5 cells/mL was introduced to the wells of a 12-well plate containing culture inserts. After incubating the cells in a complete culture medium for 24 h until they grew around the inserts, the inserts were immediately removed to create a 500 μm wide cell-free scratch. Next, the sterilized hydrogel extractions were added to each well containing the supplemented DMEM and the cells were co-cultured for 24 h. Cell morphology and distribution images were captured at different 8 h time durations between 0 and 16 h using an inverted microscope, and the relative healing rate of the scratch area was quantified using ImageJ software.

2.14. Fluorescence staining test

The hydrogel extraction solutions with NIH/3T3 cells were incubated at 37 °C in a 5 % CO_2 atmosphere. On the first and third days, the extraction solutions of the cultured cells were retrieved. After fixing the cells with 25 % glutaraldehyde, the cells were stained for viability using calcein-AM (green) and propidium iodide (red). After staining, the cells were observed using a fluorescence microscope to determine the proportion of dead and live cells [61].

2.15. Transwell migration assay

The experimental method of Transwell Migration Assay refers to previous research [62]. Initially, NIH/3T3 cells were cultured in a 5 % CO_2 atmosphere at 37 °C until they reached 90 % confluency. Washing of the cells was then undertaken with PBS, and the cells were collected by centrifugation. Subsequently, collagen or Matrigel was applied to the bottom of the membrane (cell isolation membrane) in the Transwell's upper chamber and incubated to form a solid matrix layer. Serum-free medium was added to the upper chamber, and cell concentration was adjusted to 1×10^6 cells/mL before seeding 100 μL into each upper chamber. 600 μL of the DMEM containing 10 % FBS, was then loaded in the lower chamber to function as a chemoattractant. Following the addition of the appropriate amount of hydrogel extract (4 mL extract in 10 mL DMEM), the setup was incubated for 24 h to promote cell migration into the lower chamber. At the end of the experiment, the migrated cells, through the membrane, were fixed with formaldehyde, and subsequent

staining was achieved using crystal violet, washed, and counted under a microscope to assess the particular impacts of the extracts on cell invasion capabilities.

2.16. EdU assay

Initially, NIH/3T3 cells were seeded in suitable culture dishes and cultured at 37 °C with 5 % CO_2 atmosphere until reaching the appropriate density. Subsequently, an appropriate concentration of 5-ethynyl-2′-deoxyuridine (EdU) was introduced to the medium, and cells were incubated for 6 h to incorporate EdU into newly synthesized DNA. Washing of the cells was then undertaken using PBS to eliminate any unreacted EdU after which 400 μL of 4 % formaldehyde was added and allowed to stand for 15 min. Next, the permeabilization of the cells was achieved via a 20 min treatment using 0.5 % Triton X-100 to facilitate dye penetration. A click chemistry reaction was undertaken, wherein a fluorescently labelled azide reacted with EdU to mark the newly synthesized DNA. Finally, the labelled cells were imaged and analyzed using an appropriate fluorescence microscope to quantitatively determine the proportion of cells exhibiting fluorescent labelling, thus assessing the proliferative activity of the cells [63].

2.17. Statistical analysis

The experiments were performed thrice, and results were presented as means ± standard deviation. Data were analyzed using one-way ANOVA with the SPSS 22 statistical software. Pairwise comparisons were conducted using the Bonferroni method, and statistical significance was considered at $p < 0.05$, unless otherwise noted.

3. Results and discussions

3.1. Quaternary ammonium salt modified chitosan preparation

Fig. 1a illustrates the reaction for quaternary ammonium salt modified chitosan preparation. The quaternary ammonium groups are grafted to chitosan vai a nucleophilic substitution reaction of chitosan -NH_2 groups and epoxy groups to obtain QCS, and the successful synthesis of QCS synthesis is investigated using the FT-IR spectra analysis (Fig. 1b). Fig. 1b shows that the peak at 3381 cm^{-1} in the FT-IR spectrum of chitosan indicates the presence of hydrogen bonding, with a splitting phenomenon due to hydrogen bond interactions. Additionally, a distinct absorption peak around 1592 cm^{-1} indicates to the presence of -NH_2 group. In contrast, the QCS FT-IR spectrum showed a single peak of -OH at 3354 cm^{-1}, while at 1481 cm^{-1}, a peak associated with the bending vibration of a C-H of

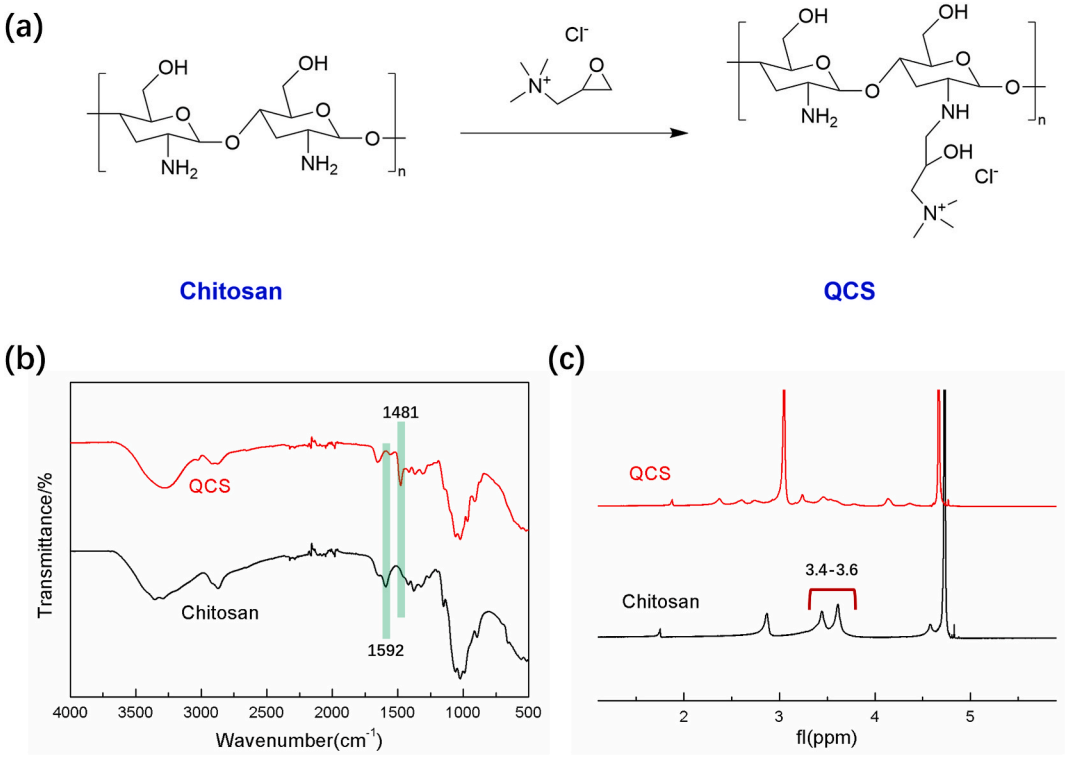

Fig. 1. (a) Schematic synthesis process of quaternary ammonium modified chitosan (QCS). (b) FT-IR spectra and (c) ^{1}H NMR spectra of chitosan and QCS.

the -CH_3 was observed. The disappearance of the peak at 1592 cm^{-1}, corresponding to the bending vibration of the primary amine N-H, indicates the occurrence of a quaternization reaction on chitosan. Furthermore, the synthesis of QCS was verified by considering the ^1H NMR spectrum (Fig. 1c). The peak of -NH_2 at δ = 3.4–3.6 ppm in the ^1H NMR spectrum of QCS disappears with the grafting reaction due to hydrogen bond interaction [64]. The obtained results of FT-IR and ^1H NMR were also consistent with the previously published works, confirming the successful synthesis of QCS [10,42].

3.2. Preparation of oxidized pullulan

Pullulan was oxidized via conversion of -CH_2OH to -CHO groups to obtain oxidized pullulan (OPL). Fig. 2a illustrates the schematic process of the reaction. Analysis of the FT-IR spectrum (Fig. 2b) reveals a new absorption peak at 1732 cm^{-1} in OPL's spectrum, indicating the formation of aldehyde groups through the oxidation reaction with sodium periodate. Additionally, in the ^1H NMR spectrum of OPL shown in Fig. 2c, absorption peaks corresponding to aldehyde groups appear between δ = 4.79–4.51 ppm, further confirming the oxidation of pullulan successfully [37,65].

3.3. Preparation of QCS/OPL hydrogels

In this work, with the regulation of the weight ratios of QCS solution and OPL solution (1:1, 4:1, and 9:1), three types of QCS/OPL hydrogels (QCS/OPL-11, QCS/OPL-41, and QCS/OPL-91) were prepared. The QCS/OPL hydrogel could be facilely fabricated by uniformly mixing QCS solution and OPL solution under room temperature conditions. The reaction mechanism involves the Schiff base reaction, where the amino groups of the QCS and the OPL's aldehyde groups form dynamic Schiff base bonds in situ (Fig. 3a) [66]. According to the FT-IR spectra of QCS/OPL hydrogels shown in Fig. 3b, the presence of a new absorption peak at 1634 cm^{-1} indicates the bending vibration of the C=N bond. This suggests that Schiff base bonds are formed in the QCS/OPL hydrogels. Furthermore, in the QCS/OPL hydrogels, the peak representing the aldehyde groups of OPL at 1732 cm^{-1} was observed to diminish or vanish, suggesting the utilization of aldehyde groups of OPL during the Schiff base reaction. Due to the Schiff base bonds, the QCS/OPL hydrogels possess self-healing abilities, which will be investigated. Furthermore, such dynamic covalent bonds give the QCS/OPL hydrogels injectable abilities. The favourable injectability of the hydrogels allows for their even dispersion onto a glass slide by applying pressure with a syringe, as shown in Fig. 3c. All QCS/OPL hydrogels display similar injectable behavior, so sample QCS/OPL-41 is displayed. In Fig. 3c, the alphabet "xy" could be easily written using the QCS/OPL hydrogel.

3.4. Microstructure of QCS/OPL hydrogels

Due to the 3D microporous structure, hydrogels have been widely used in the fields of tissue engineering and biomedicines. Fig. 3d depicts the comparable internal microstructure of the fabricated QCS/OPL hydrogels, characterized by uniform and smooth pore structures. It was clearly observed that the hydrogels with different polymer proportions displayed porous structures. Furthermore,

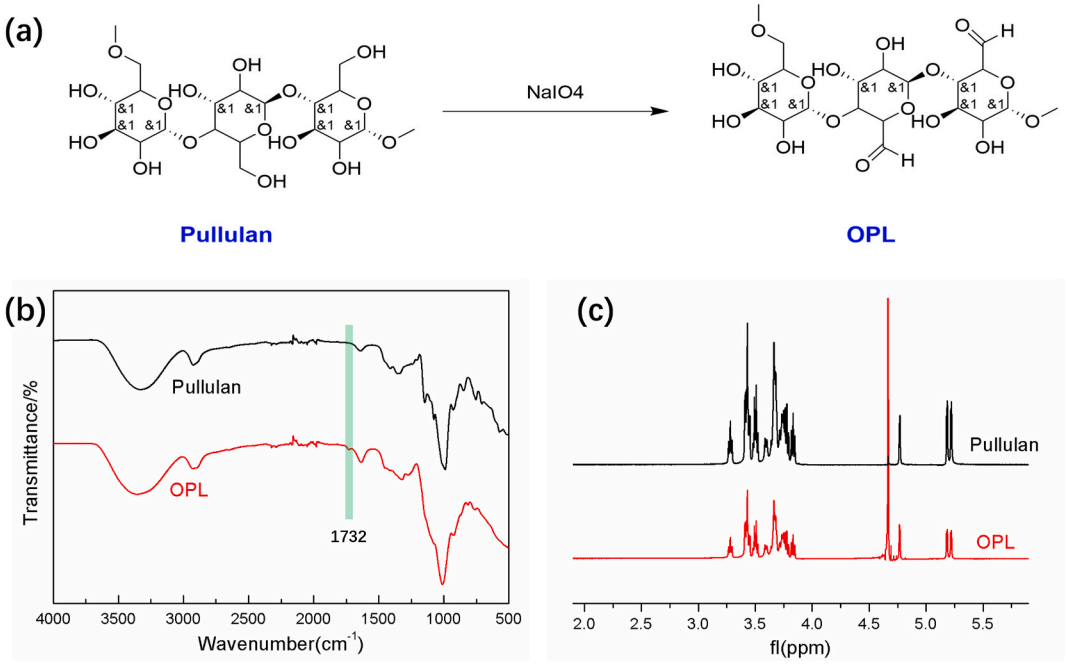

Fig. 2. (a) Schematic synthesis process of oxidized pullulan (OPL). (b) FT-IR spectra and (c) ^1H NMR spectra of pullulan and OPL.

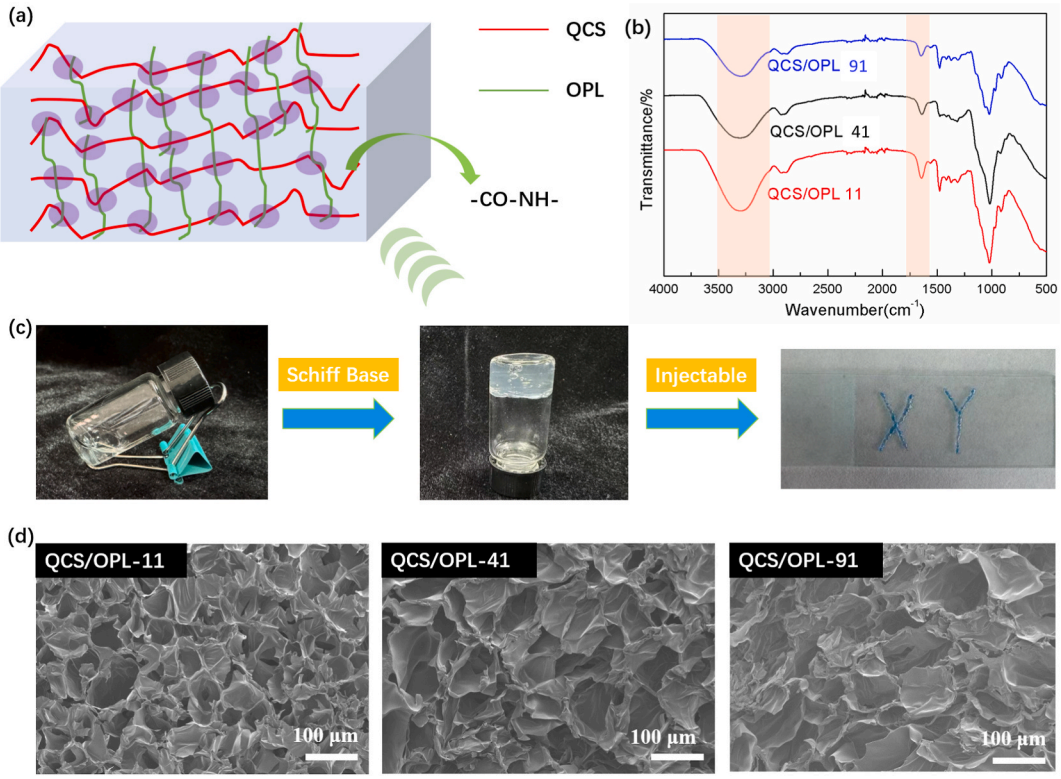

Fig. 3. (a) Schematic illustration of fabricating QCS/OPL hydrogels via Schiff base bonds crosslinking. (b) FT-IR spectra of the prepared QCS/OPL hydrogels. (c) Photos show the sol-gel transition process of QCS/OPL hydrogels under room temperature, and the obtained hydrogels could be injected using a syringe (QCS/OPL-41 as an example). (d) SEM images of the prepared QCS/OPL hydrogels.

with the increase of QCS concentration in QCS/OPL hydrogels, a slight reduction in pore size was observed, which may be attributed to the increased degree of crosslinking between amino and aldehyde groups for a denser three-dimensional network structure. With the increase of crosslinking points in the hydrogels, a much more dense 3D network structure would be formed. The uniform microstructure facilitates the transportation of more nutrients and metabolites in the hydrogels, proving the potential as wound dressings in wound healing applications [67].

3.5. Swelling properties of QCS/OPL hydrogels

The water absorption capability facilitates the application of hydrogels in wound dressings. Thus, the maximum water absorption (equilibrium swelling ratio) of QCS/OPL hydrogels is investigated, as shown in Fig. 4a and **b**. It is shown that the QCS/OPL hydrogels reached their maximum water absorption within 5 h, with nearly a 50-fold increase in water absorption within 30 min (Fig. 4a). Furthermore, as indicated in Fig. 4b, there were no significant differences in equilibrium water absorption rates among the three hydrogel materials, all achieving water absorption levels exceeding 200 times their original mass. Compared to our previously reported QCS based hydrogels, the hydrogels based on QCS and OPL display significant water absorption ability [10,42,44,45].

3.6. Self-healing ability of QCS/OPL hydrogels

The self-healing properties of QCS/OPL 11 hydrogel, QCS/OPL 41 hydrogel, and QCS/OPL 91 hydrogel were confirmed using a TA rheometer. Fig. 4c shows that the collapse of the hydrogel network structure occurred at 620 % strain. However at a strain of 100 %, $G'' > G'$, indicating the hydrogel's network structure was maintained. Fig. 4c shows that as G' decreased to a certain value, G' surpassed G'', leading to hydrogel network structure collapse. Notably, when subjected to a 1 % strain, the hydrogel's G' quickly reverted to its original value. Results from cyclic tests demonstrated the hydrogel network's ability to undergo repetitive repairs, attributed to the Schiff base dynamic bonds formed between the amino groups and aldehyde groups on QCS and OPL, respectively, which provide the QCS/OPL hydrogel with exceptional self-healing properties. In addition, QCS/OPL 11 hydrogel was chosen as a representative to demonstrate the macroscopic self-healing capability of the hydrogel. The hydrogel was first cut into two equal halves in the macroscopic self-healing test. Staining of one-half of the hydrogel with methylene blue was undertaken, while the other half was left unstained. Afterwards, the two halves were contacted. As depicted in Fig. 4d, after 9 min, the hydrogel successfully underwent self-healing under room temperature conditions. When one end was gripped with forceps and held vertically, the healed hydrogel did

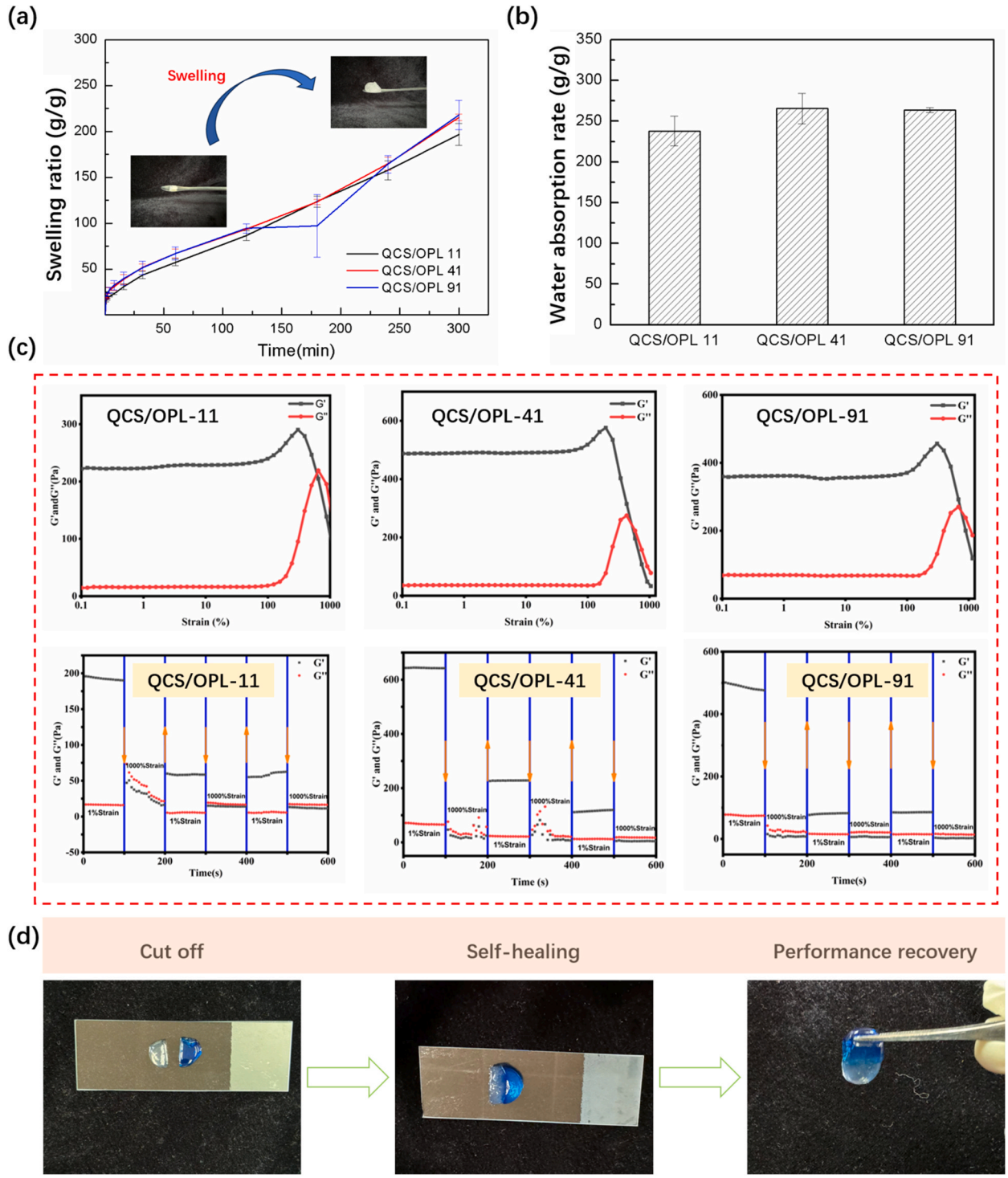

Fig. 4. (a) The swelling properties and (b) water absorption capacity of the prepared QCS/OPL hydrogels are shown, with images in (a) illustrating the water-absorbed samples at various times (QCS/OPL-41 as an example). (c) The storage modulus (G') and loss modulus (G'') of the QCS/OPL hydrogels under strain are presented. Additionally, the self-healing capability was assessed through rheological analysis, where G' and G'' were recorded over time using alternating 1 % and 100 % strain. (d) Photos demonstrating the self-healing performance of the prepared QCS/OPL hydrogels, with QCS/OPL-41 shown as an example.

not detach, showcasing the outstanding self-healing ability of the QCS/OPL hydrogel.

3.7. Adhesive properties of QCS/OPL hydrogel

Fig. 5 highlights the adhesion performances of QCS/OPL hydrogels with favourable adhesion to surfaces of various materials, such as human skin, metal, plastic, rubber, and glass (Fig. 5a). Polysaccharide-based hydrogels' adhesion performance primarily comprises physical, chemical, electrostatic, and wetting adhesion. Hydrogels are highly hydrated soft materials involving physical capillary and wetting adhesion [68,69]. Additionally, the quaternary ammonium cations in the QCS/OPL hydrogel can form an electrostatic attraction with opposite charges on the adhered surface, achieving electrostatic adhesion [70]. The hydroxyl groups and other functionalities in the polysaccharide chains can bond with polar groups on the target surface using hydrogen bonds, thereby providing additional adhesion force [71]. The detailed adhesion mechanism is illustrated in Fig. 5b.

3.8. Antibacterial properties of QCS/OPL hydrogel

The antibacterial performance of QCS/OPL hydrogel is illustrated in Fig. 6a and **b**. The results show that the solution becomes more transparent with reduced bacterial content after the co-cultivation *E. coli* and *S. aureus* with the QCS/OPL hydrogel samples. This indicates a significant inhibitory effect of QCS/OPL hydrogels of different proportions on *E. coli* and *S. aureus* proliferation [72]. Furthermore, the antibacterial effect of QCS/OPL hydrogels is inversely proportional to OD_{600}. Through measurement of the solution's OD_{600}, it was found that QCS/OPL 11 hydrogel and QCS/OPL 41 hydrogel exhibited better inhibitory impact on *S. aureus* than on *E. coli*. The cationic properties of the quaternary ammonium groups attached to chitosan polymers allow them to interact with the negative charges on bacterial cell walls, leading to structural destruction of the cell membrane that impairs cell viability and growth [73]. Moreover, oxidized Prussian polysaccharide possesses oxidative properties, producing reactive oxygen species (ROS) in bacterial

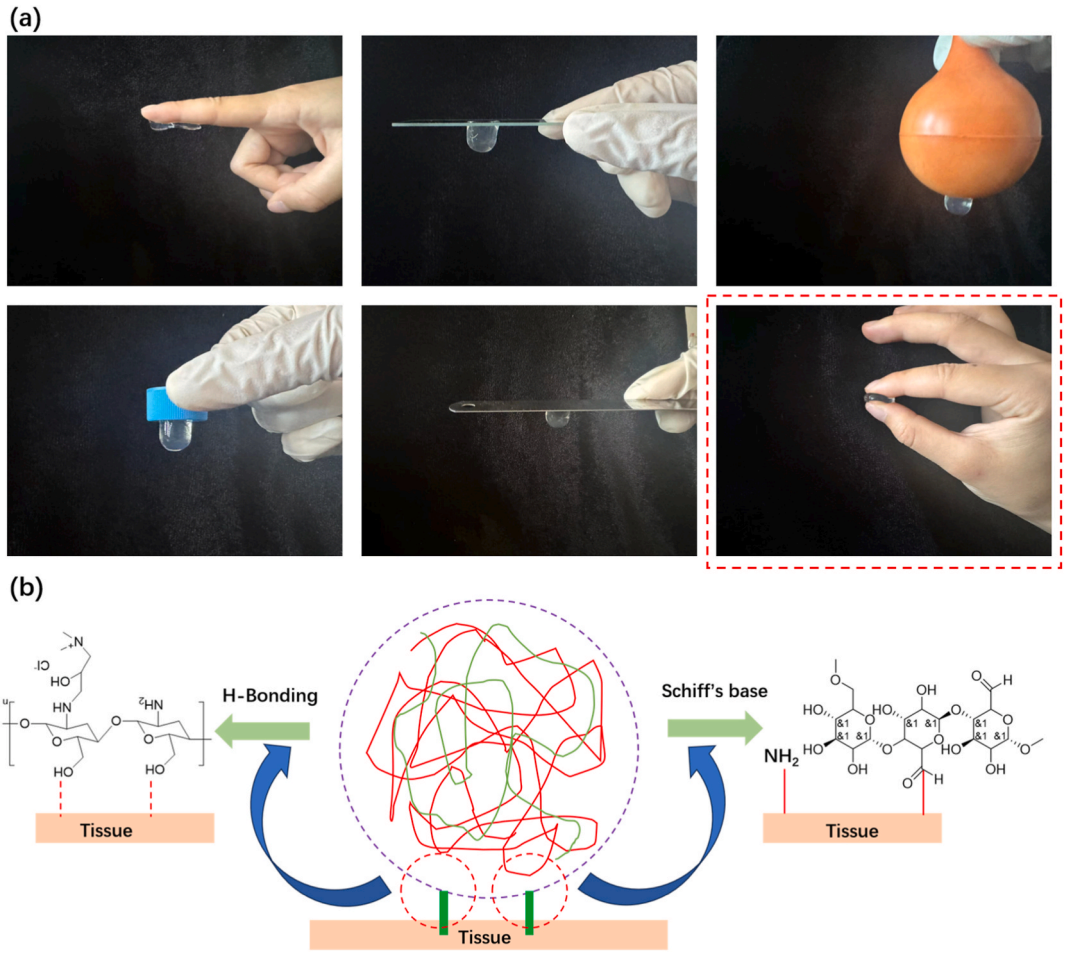

Fig. 5. (a) The prepared QCS/OPL hydrogels depict the adhesive properties, with representative images showcasing adhesion to various surfaces. Furthermore, the hydrogels could be compressed using fingers. Sample QCS/OPL-41 was only displayed, and all hydrogels obtained had the same performance. (b) The possible adhesive mechanism was illustrated.

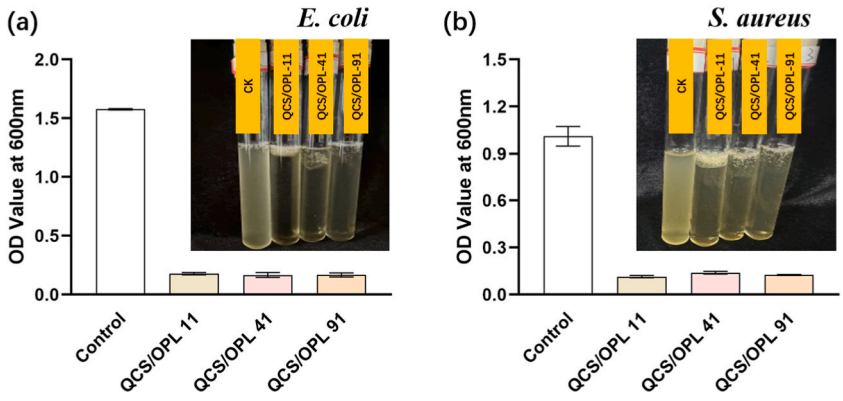

Fig. 6. The antibacterial performances of the QCS/OPL hydrogels against (a) *E. coli* and (b) *S. aureus* in LB agar liquid medium for 6 h, and the photos inserted were the hydrogels in LB agar liquid medium.

cells. These ROS cause oxidative damage to cellular structures, further impeding bacterial growth and reproduction. Overall, through a synergistic mechanism involving the disruption of membranes of cells, as well as the induction of oxidative stress, QCS/OPL hydrogels exhibit notable antibacterial effects against both *E. coli* and *S. aureus*. Such antibacterial characteristics render the material valuable for medical, food packaging, and water treatment applications.

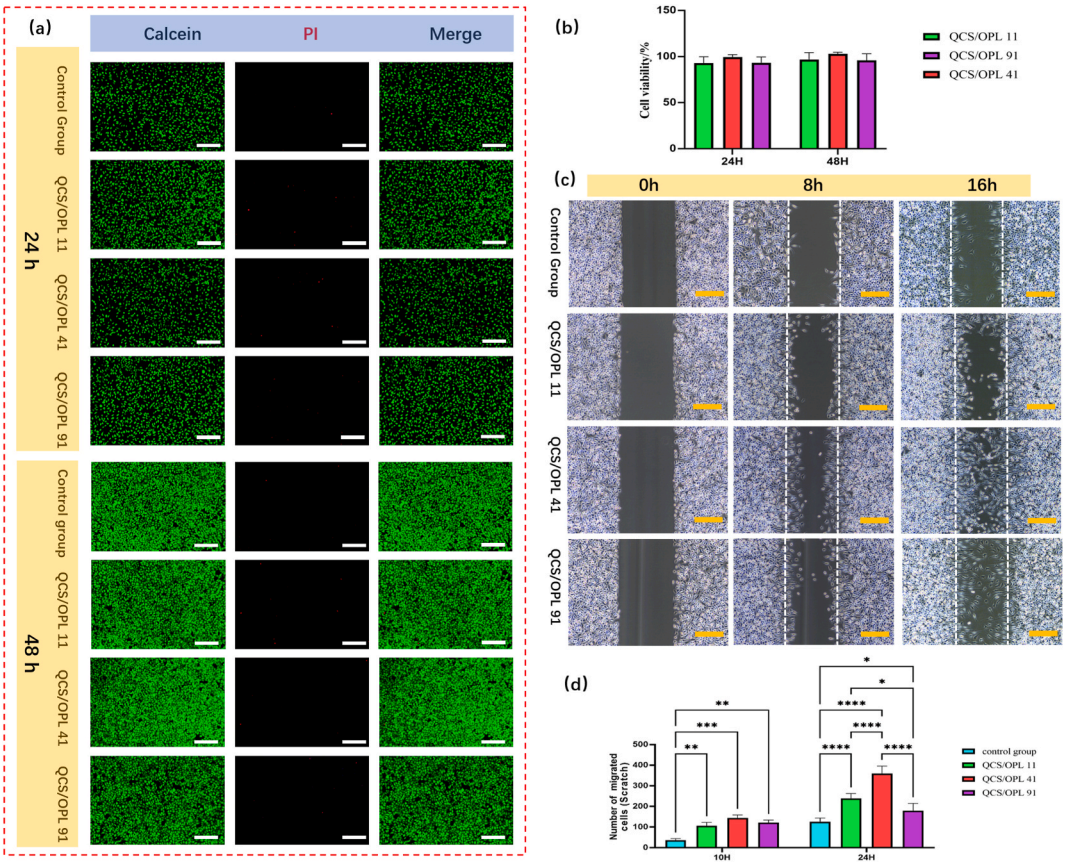

Fig. 7. (a) Live/Dead (Calcein/PI) staining of NIH/3T3 cells co-cultured with QCS/OPL hydrogels for 24 and 48 h, where live cells appear green and dead cells appear red (b) CCK-8 assay was further employed to investigate the cytocompatibilities of the co-cultured QCS/OPL hydrogels with NIH/3T3 cells. (c) NIH/3T3 cells scratch results at 8 and 16 h. (d) Statistical analysis of cell migration. The white scale and yellow bars represent 100 μm. (For interpretation of the references to color in this figure legend, the reader is referred to the Web version of this article.)

3.9. Co-culture of cells with QCS/OPL hydrogels

Biocompatibilities of the hydrogels were assessed using QCS/OPL hydrogel samples co-cultured with skin fibroblasts. The results, as shown in Fig. 7a and b, indicate that all hydrogel samples exhibited good biocompatibility. A comparison of the data between 24 h and 48 h reveals significant cell proliferation over time with no apparent cell death observed. The CCK-8 statistical data further confirmed the biocompatibility of the QCS/OPL hydrogel materials, with cell viability rates exceeding 95 % for all samples. The cell migration ability was evaluated to further assess the impact of the hydrogel materials on skin fibroblasts. As depicted in Fig. 7c, analysis of the experimental results shows that, in comparison to the data at 8 h and 16 h, the hydrogel groups demonstrated efficient cell migration through prolonged co-culture. Specifically, the QCS/OPL 41 hydrogel group exhibited the highest migration efficiency. Fig. 7d provides further statistical analysis, indicating that the cell migration counts for QCS/OPL 41 at 16 h reached approximately 350 cells, higher than the approximately 200 cells for QCS/OPL 11 and approximately 150 cells for QCS/OPL 91 hydrogel groups. The biocompatibility and structure of the materials primarily determine the migration of cells. All three types of QCS/OPL hydrogels used were biocompatible natural polymeric materials. SEM microstructural results (Fig. 3d) revealed that the QCS/OPL 41 samples had the optimal pore structure, which is more conducive to cell crawling, thus demonstrating superior migration capability.

To further determine the effects of hydrogel materials on cellular activity, QCS/OPL hydrogel samples were co-cultured with cells. The DNA synthesis during cell proliferation and the Transwell cell invasion capabilities were characterized, with results presented in Fig. 8. Analysis from Fig. 8a indicates significant DNA synthesis occurring after 6 h of culture, where the hydrogel groups notably outperformed the control group. Further statistical analysis, as shown in Fig. 8b, demonstrates that the QCS/OPL 41 hydrogel group had a ratio of newly formed cells to initial cells exceeding 40 %. Fig. 8c and **d** also show the cell invasion capabilities of the hydrogels with the QCS/OPL 91 hydrogel group shown to notably enhance cell invasion capabilities to a greater extent compared to other hydrogel groups and the control group. Statistical analysis further indicates that the number of cells migrating through the membrane materials in the QCS/OPL 91 group was approximately 1500, while other hydrogel groups ranged between 500 and 800. In contrast, the blank control group had fewer than 500 cells passing through.

4. Conclusion

The present study investigated functional QCS/OPL hydrogels that were synthesized through the Schiff base reaction between chitosan quaternary ammonium salt, and oxidized pullulan. All obtained QCS/OPL hydrogels exhibited a consistent porous structure, with pores conducive to storing nutrients, drugs, and metabolic products while simultaneously providing an attachment environment for cell growth. The QCS/OPL hydrogels demonstrated good adhesion on various surfaces, thus may prevent detachment from wounds. Furthermore, the QCS/OPL hydrogels exhibit favourable mechanical properties and self-healing capabilities, which are essential for tissue regeneration. The QCS/OPL hydrogel also demonstrated swelling properties, making it well-suited as a wound dressing capable of absorbing contaminants discharged from wounds. In addition, the QCS/OPL hydrogel showed favourable antibacterial activity against both *E. coli* and *S. aureus*. Cell compatibility tests revealed that the QCS/OPL hydrogels had no cytotoxicity to cell growth. Based on these physicochemical properties, QCS/OPL hydrogel has potential in biomedical materials.

Ethics statement

The cells (NIH/3T3 cells, CRL-1658™) used in this paper were obtained from ATCC company.

Conflicts of competing interest

The authors declare no competing financial interest.

Data availability

Data will be made available on request.

CRediT authorship contribution statement

Qian He: Writing – review & editing, Writing – original draft, Supervision, Formal analysis, Data curation. **Xiaoyue Ding:** Writing – original draft, Visualization, Formal analysis, Data curation, Conceptualization. **Jun Deng:** Writing – review & editing, Resources, Formal analysis, Conceptualization. **Yanze Zhang:** Writing – review & editing, Investigation, Formal analysis, Data curation. **Xiaoyi Wang:** Writing – review & editing, Formal analysis. **Dan Zhan:** Writing – review & editing, Formal analysis. **Oseweuba Valentine Okoro:** Writing – review & editing, Writing – original draft, Formal analysis. **Lizhao Yan:** Writing – review & editing, Writing – original draft, Validation, Formal analysis, Data curation. **Armin Shavandi:** Writing – review & editing. **Lei Nie:** Writing – review & editing, Writing – original draft, Supervision, Resources, Funding acquisition, Formal analysis, Data curation, Conceptualization.

Declaration of competing interest

The authors declare that they have no known competing financial interests or personal relationships that could have appeared to

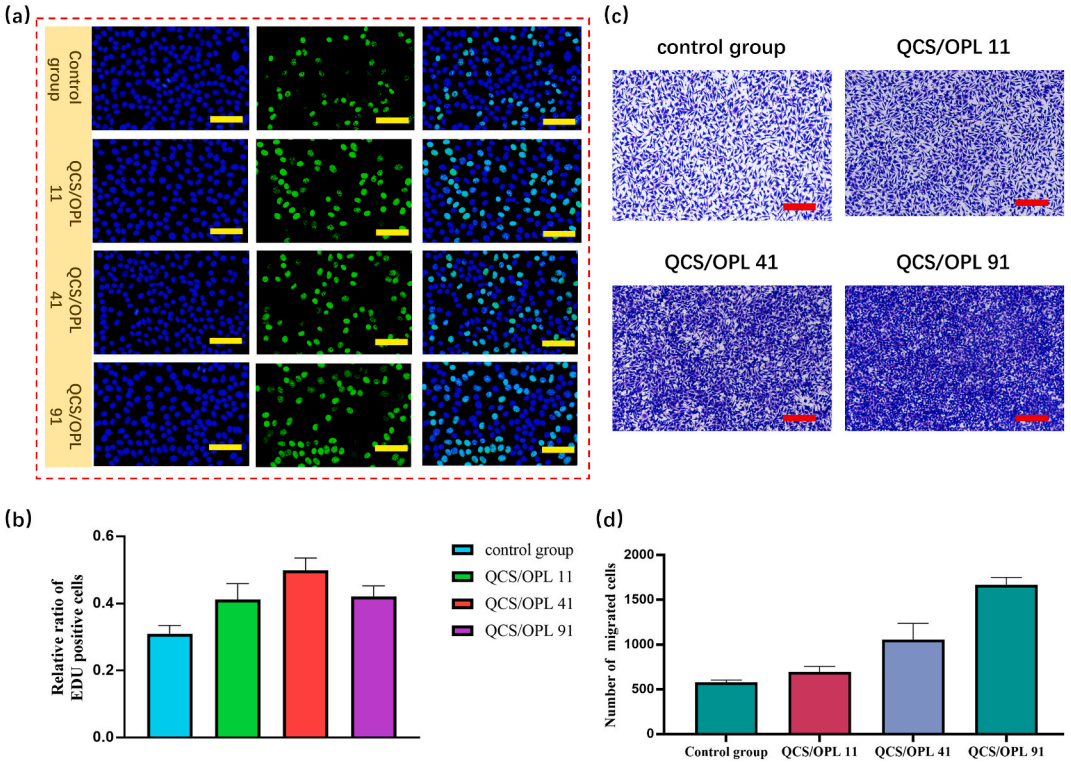

Fig. 8. (a) NIH/3T3 cells proliferation staining (Hoechst); initial cells are stained blue, and newly formed cells are stained green. (b) Analysis of the ratio of newly formed cells to initial cells. (c) Staining test (crystal violet) for cell migration through membrane materials. (d) Quantitative analysis of cells migrating through membrane materials; the yellow scale bar represents 25 μm, and the red scale bar represents 100 μm. (For interpretation of the references to color in this figure legend, the reader is referred to the Web version of this article.)

influence the work reported in this paper.

Acknowledgments

This research was supported by the Natural Science Foundation of Henan Province (242300421338), and Guidance Project of the Hubei Provincial Health Commission (WJ2023F035).

References

[1] S. Laquerbe, J. Es Sayed, C. Lorthioir, C. Meyer, T. Narita, G. Ducouret, P. Perrin, N. Sanson, Supramolecular crosslinked hydrogels: similarities and differences with chemically crosslinked hydrogels, Macromolecules 56 (18) (2023) 7406–7418.
[2] W. Chen, C. Zhang, S. Peng, Y. Lin, Z. Ye, Hydrogels in dental medicine, Advanced Therapeutics 7 (2023) 2300128.
[3] Z. Xiao, Q. Li, H. Liu, Q. Zhao, Y. Niu, D. Zhao, Adhesion mechanism and application progress of hydrogels, Eur. Polym. J. 173 (2022) 1112777.
[4] S. Correa, A.K. Grosskopf, H. Lopez Hernandez, D. Chan, A.C. Yu, L.M. Stapleton, E.A. Appel, Translational applications of hydrogels, Chem. Rev. 121 (18) (2021) 11385–11457.
[5] L. Nie, J. Li, G. Lu, X. Wei, Y. Deng, S. Liu, S. Zhong, Q. Shi, R. Hou, Y. Sun, Temperature responsive hydrogel for cells encapsulation based on graphene oxide reinforced poly (N-isopropylacrylamide)/hydroxyethyl-chitosan, Mater. Today Commun. 31 (2022) 103697.
[6] B. Zhuang, T. Chen, Z. Xiao, Y. Jin, Drug-loaded implantable surgical cavity-adaptive hydrogels for prevention of local tumor recurrence, Int. J. Pharm. 577 (2020) 119048.
[7] P. Bertsch, M. Diba, D.J. Mooney, S.C.G. Leeuwenburgh, Self-healing injectable hydrogels for tissue regeneration, Chem. Rev. 123 (2) (2023) 834–873.
[8] K.J. De France, E.D. Cranston, T. Hoare, Mechanically reinforced injectable hydrogels, ACS Appl. Polym. Mater. 2 (3) (2020) 1016–1030.
[9] O. Jeznach, D. Kołbuk, P. Sajkiewicz, Injectable hydrogels and nanocomposite hydrogels for cartilage regeneration, J. Biomed. Mater. Res. 106 (10) (2018) 2762–2776.
[10] W. Guo, X. Gao, X. Ding, P. Ding, Y. Han, Q. Guo, Y. Ma, O.V. Okoro, Y. Sun, G. Jiang, Self-adhesive and self-healing hydrogel dressings based on quaternary ammonium chitosan and host-guest interacted silk fibroin, Colloids Surf. A Physicochem. Eng. Asp. (2024) 133145.
[11] H. Xuan, S. Wu, S. Fei, B. Li, Y. Yang, H. Yuan, Injectable nanofiber-polysaccharide self-healing hydrogels for wound healing, Mater. Sci. Eng., C 128 (2021).
[12] S. Guan, K. Zhang, L. Cui, J. Liang, J. Li, F. Guan, Injectable gelatin/oxidized dextran hydrogel loaded with apocynin for skin tissue regeneration, Biomater. Adv. 133 (2022).
[13] S. Correa, A.K. Grosskopf, H. Lopez Hernandez, D. Chan, A.C. Yu, L.M. Stapleton, E.A. Appel, Translational applications of hydrogels, Chem. Rev. 121 (2021) 11385–11457.
[14] C. Mortier, D.C.S. Costa, M.B. Oliveira, H.J. Haugen, S.P. Lyngstadaas, J.J. Blaker, J.F. Mano, Advanced hydrogels based on natural macromolecules: chemical routes to achieve mechanical versatility, Mater. Today Chem. 26 (2022) 101222.
[15] Q. Zhao, Y. Chen, Y. Liu, A polysaccharide/tetraphenylethylene-mediated blue-light emissive and injectable supramolecular hydrogel, Chin. Chem. Lett. 29 (1) (2018) 84–86.

[16] C. Qian, T. Zhang, J. Gravesande, C. Baysah, X. Song, J. Xing, Injectable and self-healing polysaccharide-based hydrogel for pH-responsive drug release, Int. J. Biol. Macromol. 123 (2019) 140–148.
[17] P. Ding, X. Ding, J. Li, W. Guo, O.V. Okoro, M. Mirzaei, Y. Sun, G. Jiang, A. Shavandi, L. Nie, Facile preparation of self-healing hydrogels based on chitosan and PVA with the incorporation of curcumin-loaded micelles for wound dressings, Biomed. Mater. 19 (2024) 025021.
[18] P. Ding, O.V. Okoro, Y. Sun, L. Wang, X. Wei, S. Liu, Y. Deng, L. Fan, G. Jiang, L. Wang, A. Shavandi, L. Nie, Graphene oxide-reinforced alginate/gelatin hydrogel via Schiff-base bond and thiol-Michael addition for bone regeneration, Mater. Today Commun. 33 (2022) 104904.
[19] F. Gao, C. Jiao, B. Yu, H. Cong, Y. Shen, Preparation and biomedical application of injectable hydrogels, Mater. Chem. Front. 5 (2021) 4912–4936.
[20] Y. Sun, D. Nan, H. Jin, X. Qu, Recent advances of injectable hydrogels for drug delivery and tissue engineering applications, Polym. Test. 81 (2020) 106283.
[21] K. Wang, Z. Han, Injectable hydrogels for ophthalmic applications, J. Contr. Release 268 (2017) 212–224.
[22] H. Ding, J. Liu, P. Huo, R. Ding, X. Shen, H. Mao, Y. Wen, H. Li, Z.L. Wu, Ultra-stretchable and conductive polyacrylamide/carboxymethyl chitosan composite hydrogels with low modulus and fast self-recoverability as flexible strain sensors, Int. J. Biol. Macromol. 253 (2023) 127146.
[23] J. Seo, S. Oh, G. Choi, H.S. Lee, Anti-dryable, anti-freezable, and self-healable conductive hydrogel for adhesive electrodes, Compos. Interfac. 29 (13) (2022) 1561–1571.
[24] L. Wu, G. Chen, Z. Li, Layered rare-earth hydroxide/polyacrylamide nanocomposite hydrogels with highly tunable photoluminescence, Small 13 (23) (2017) 1604070.
[25] T.-C. Sun, B.-Y. Yan, X.-C. Ning, Z.-Y. Tang, C. Hui, M.-z. Hu, S. Ramakrishna, Y.-Z. Long, J. Zhang, A nanofiber hydrogel derived entirely from ocean biomass for wound healing, Nanoscale Adv 5 (2023) 160–170.
[26] X. Zhang, G.J. Kim, M.G. Kang, J.K. Lee, J.W. Seo, J.T. Do, K. Hong, J.M. Cha, S.R. Shin, H. Bae, Marine biomaterial-based bioinks for generating 3D printed tissue constructs, Mar. Drugs 16 (12) (2018) 484.
[27] A.S. Sumayya, G. Muraleedhara Kurup, Marine macromolecules cross-linked hydrogel scaffolds as physiochemically and biologically favorable entities for tissue engineering applications, Journal of Biomaterials Science 28 (9) (2017) 807–825. Polymer Edition.
[28] S. Liu, Y. Zhao, H. Wei, L. Nie, P. Ding, H. Sun, Y. Guo, T. Chen, O.V. Okoro, A. Shavandi, Injectable hydrogels based on silk fibroin peptide grafted hydroxypropyl chitosan and oxidized microcrystalline cellulose for scarless wound healing, Colloids Surf. A Physicochem. Eng. Asp. 647 (2022) 129062.
[29] Natália Maria B Ladeira, Claudio L. Donnici, Mesquita João Paulo de, V. Fabiano Pereira, Preparation and characterization of hydrogels obtained from chitosan and carboxymethyl chitosan, J. Polym. Res. 28 (2021) 335.
[30] S.-P. Lin, K.-Y. Lo, T.-N. Tseng, J.-M. Liu, T.-Y. Shih, K.-C. Cheng, Evaluation of PVA/dextran/chitosan hydrogel for wound dressing, Cell. Polym. 38 (11) (2019) 026248931983921.
[31] S. Peers, A. Montembault, C. Ladavière, Chitosan hydrogels for sustained drug delivery, J. Contr. Release 326 (2020) 150–163.
[32] O.V. Okoro, L. Nie, O. Gunduz, S. Ulag, M. Hamidi, A. Shavandi, Technoeconomic assessment of biopolymer production from Crustacean waste with the UK as a, Case Study 15 (2023) 2280.
[33] Z. Chen, X. Yao, L. Liu, J. Guan, M. Liu, Z. Li, J. Yang, S. Huang, J. Wu, F. Tian, M. Jing, Blood coagulation evaluation of N-alkylated chitosan, Carbohydr. Polym. 173 (2017) 259–268.
[34] A. Piegat, A. Żywicka, A. Niemczyk, A. Goszczyńska, Antibacterial activity of N, O-acylated chitosan derivative, Polymers 13 (2020) 107.
[35] Z. Sun, C. Shi, X. Wang, Q. Fang, J. Huang, Synthesis, characterization, and antimicrobial activities of sulfonated chitosan, Carbohydr. Polym. 155 (2017) 321–328.
[36] K. Asadi, R. Heidari, M. Hamidi, M.M. Ommati, S. Yousefzadeh-Chabok, N. Samiraninezhad, M. Khoshneviszadeh, M. Hashemzaei, A. Gholami, Trinitroglycerin-loaded chitosan nanogels: shedding light on cytotoxicity, antioxidativity, and antibacterial activities, Int. J. Biol. Macromol. 265 (2024) 130654, 130654.
[37] Du H., Parit M., Liu K., Zhang M., Jiang Z., Huang T.-S., Zhang X., Si C., Engineering cellulose nanopaper with water resistant, antibacterial, and improved barrier properties by impregnation of chitosan and the followed halogenation, Carbohydr. Polym. 270 (2021) 118372.
[38] S. Thanakkasaranee, K. Jantanasakulwong, Y. Phimolsiripol, N. Leksawasdi, P. Seesuriyachan, T. Chaiyaso, P. Jantrawut, W. Ruksiriwanich, S. Rose Sommano, W. Punyodom, A. Reungsang, T.M.P. Ngo, P. Thipchai, W. Tongdeesoontorn, P. Rachtanapun, High substitution synthesis of carboxymethyl chitosan for properties improvement of carboxymethyl chitosan films depending on particle sizes, Molecules 26 (19) (2021) 6013.
[39] L. Fan, S. Zou, H. Ge, Y. Xiao, H. Wen, H. Feng, M. Liu, M. Nie, Preparation and characterization of hydroxypropyl chitosan modified with collagen peptide, Int. J. Biol. Macromol. 93 (2016) 636–643.
[40] B.-I. Andreica, X. Cheng, L. Marin, Quaternary ammonium salts of chitosan. A critical overview on the synthesis and properties generated by quaternization, Eur. Polym. J. 139 (2020) 110016.
[41] Q. Wu, L. Wang, P. Ding, Y. Deng, O.V. Okoro, A. Shavandi, L. Nie, Mercaptolated chitosan/methacrylate gelatin composite hydrogel for potential wound healing applications, Compos. Commun. 35 (2022) 101344.
[42] L. Nie, Q. Wei, M. Sun, P. Ding, L. Wang, Y. Sun, X. Ding, O.V. Okoro, G. Jiang, A. Shavandi, Injectable, self-healing, transparent, and antibacterial hydrogels based on chitosan and dextran for wound dressings, Int. J. Biol. Macromol. 233 (2023) 123494.
[43] W. Guo, X. Ding, H. Zhang, Z. Liu, Y. Han, Q. Wei, O.V. Okoro, A. Shavandi, L. Nie, Recent advances of chitosan-based hydrogels for skin-wound dressings, Gels 10 (2024) 175.
[44] L. Wang, X. Ding, J. Li, M. Li, P. Ding, W. Guo, Q. Wu, Y. Sun, G. Jiang, O.V. Okoro, M. Mirzaei, A. Shavandi, L. Fan, L. Nie, Genipin crosslinked quaternary ammonium chitosan hydrogels for wound dressings, Biomed. Mater. 19 (2024) 045042.
[45] J. Deng, J. Li, L. Yan, W. Guo, X. Ding, P. Ding, S. Liu, Y. Sun, G. Jiang, O.V. Okoro, A. Shavandi, Z. Xie, L. Fan, L. Nie, Accelerated, injectable, self-healing, scarless wound dressings using rGO reinforced dextran/chitosan hydrogels incorporated with PDA-loaded asiaticoside, Int. J. Biol. Macromol. 278 (2024) 134424.
[46] Y. Ma, X. Zhou, Z. Mo, Q. Zhou, B. Hui, Z. Cai, X. Wang, H. Li, S. Tang, Quaternary ammonium carboxymethyl chitosan composite hydrogel with efficient antibacterial and antioxidant properties for promoting wound healing, Int. J. Biol. Macromol. 268 (2024) 131871.
[47] R.S. Singh, N. Kaur, D. Singh, S.S. Purewal, J.F. Kennedy, Pullulan in pharmaceutical and cosmeceutical formulations: a review, Int. J. Biol. Macromol. 231 (2023) 123353.
[48] F. Aghajannataj Ahangarkola, G. Najafpour-Darzi, R. Ramezani Kalmer, Towards a novel pullulan and pullulan-enteric hard capsules: study of drug release and crucial capsule features, J. Drug Deliv. Sci. Technol. 92 (2024) 105297.
[49] M. Rai, M. Wypij, A.P. Ingle, J. Trzcińska-Wencel, P. Golińska, Emerging trends in pullulan-based antimicrobial systems for various applications, Int. J. Mol. Sci. 22 (24) (2021) 13596.
[50] C.K. de Souza, T. Ghosh, N. Lukhmana, S. Tahiliani, R. Priyadarshi, T.G. Hoffmann, S.D. Purohit, S.S. Han, Pullulan as a sustainable biopolymer for versatile applications: a review, Mater. Today Commun. 36 (2023) 106477.
[51] Li S., Fan M., Deng S., Tao N., Characterization and application in packaging grease of gelatin–sodium alginate edible films cross-linked by pullulan, Polymers.14 (15) (2022) 3199.
[52] S. Roy, M. Halder, P. Ramprasad, S. Dasgupta, Y. Singh, D. Pal, Oxidized pullulan exhibits potent antibacterial activity against S. aureus by disrupting its membrane integrity, Int. J. Biol. Macromol. 249 (2023) 126049.
[53] L. Nian, Y. Xie, X. Sun, M. Wang, C. Cao, Chitosan quaternary ammonium salt/gelatin-based biopolymer film with multifunctional preservation for perishable products, Int. J. Biol. Macromol. 228 (2023) 286–298.
[54] W. Zheng, Z. Zhang, Y. Li, L. Wang, F. Fu, H. Diao, X. Liu, A novel pullulan oxidation approach to preparing a shape memory sponge with rapid reaction capability for massive hemorrhage, Chem. Eng. J. 447 (2022).
[55] D.M. Suflet, M. Constantin, I.M. Pelin, I. Popescu, C.M. Rimbu, C.E. Horhogea, G. Fundueanu, Chitosan–oxidized pullulan hydrogels loaded with essential clove oil: synthesis, characterization, antioxidant and antimicrobial properties, Gels 10 (4) (2024) 227.
[56] S. Liu, Y. Zhao, M. Li, L. Nie, Q. Wei, O. Valentine Okoro, H. Jafari, S. Wang, J. Deng, J. Chen, A. Shavandi, L. Fan, Bioactive wound dressing based on decellularized tendon and GelMA with incorporation of PDA-loaded asiaticoside nanoparticles for scarless wound healing, Chem. Eng. J. 466 (2023) 143016.

[57] B.-I. Andreica, L. Mititelu-Tartau, I. Rosca, I.M. Pelin, E. Nicol, L. Marin, Biocompatible hydrogels based on quaternary ammonium salts of chitosan with high antimicrobial activity as biocidal agents for disinfection, Carbohydr. Polym. 342 (2024) 122389.
[58] G. Bhardwaj, T.J. Webster, Increased NIH 3T3 fibroblast functions on cell culture dishes which mimic the nanometer fibers of natural tissues, Int. J. Nanomed. 10 (1) (2015) 5293–5299.
[59] L. Cai, X. Qin, Z. Xu, Y. Song, H. Jiang, Y. Wu, H. Ruan, J. Chen, Comparison of cytotoxicity evaluation of anticancer drugs between real-time cell analysis and CCK-8 method, ACS Omega 4 (2019) 12036–12042.
[60] L. Yan, S. Liu, J. Wang, X. Ding, Y. Zhao, N. Gao, Z. Xia, M. Li, Q. Wei, O.V. Okoro, Y. Sun, L. Nie, A. Shavandi, G. Jiang, J. Chen, L. Fan, Y. Weng, Constructing nerve guidance conduit using dECM-doped conductive hydrogel to promote peripheral nerve regeneration, Adv. Funct. Mater. 34 (38) (2024) 2402698.
[61] T. Leavitt, M.S. Hu, M.T. Longaker, Isolation of live fibroblasts by fluorescence-activated cell sorting, Methods Mol. Biol. 1627 (2017) 205–212.
[62] E. Primiceri, M.S. Chiriacò, F. Dioguardi, A.G. Monteduro, E. D'Amone, R. Rinaldi, G. Giannelli, G. Maruccio, Automatic transwell assay by an EIS cell chip to monitor cell migration, Lab Chip 11 (2011) 4081–4086.
[63] X. Yin, H. Tsukaya, A pulse-chase strategy for EdU labelling assay is able to rapidly quantify cell division orientation, New Phytol. 211 (2016) 1462–1469.
[64] E. Oyervides-Muñoz, L. Avérous, G.d.J. Sosa-Santillán, E. Pollet, N.V. Pérez-Aguilar, C.M. Rojas-Caldera, J.G. Fuentes-Avilés, C. García-Astrain, EDC-mediated grafting of quaternary ammonium salts onto chitosan for antibacterial and thermal properties improvement, Macromol. Chem. Phys. 220 (2019) 1800530.
[65] K. Yin, J. Wu, Q. Deng, Z. Wu, T. Wu, Z. Luo, J. Jiang, J.-A. Duan, Tailoring micro/nanostructured porous polytetrafluoroethylene surfaces for dual-reversible transition of wettability and transmittance, Chem. Eng. J. 434 (2022) 134756.
[66] F. Guo, Y. Liu, S. Chen, Y. Lin, Y. Yue, A Schiff base hydrogel dressing loading extracts from Periplaneta Americana for diabetic wound healing, Int. J. Biol. Macromol. 230 (2023) 123256.
[67] S. Liu, Y. Zhao, M. Li, L. Nie, Q. Wei, O.V. Okoro, H. Jafari, S. Wang, J. Deng, J. Chen, Bioactive wound dressing based on decellularized tendon and GelMA with incorporation of PDA-loaded asiaticoside nanoparticles for scarless wound healing, Chem. Eng. J. 466 (2023) 143016.
[68] W.H. Kim, Y. Han, I.S. Lee, N.-I. Won, Y.H. Na, Development of hydrogel adhesion system for propagation of aquatic organisms, Polymer 255 (2022) 125112.
[69] J. Yang, R. Bai, B. Chen, Z. Suo, Hydrogel adhesion: a supramolecular synergy of chemistry, topology, and mechanics, Adv. Funct. Mater. 30 (2) (2019) 1901693.
[70] S. Liu, L. Wan, F. Hu, Z. Wen, M. Cao, F. Ai, Self-adhesive, antifreezing, and antidrying conductive glycerin/polyacrylamide/chitosan quaternary ammonium salt composite hydrogel as a flexible strain sensor, ACS Appl. Polym. Mater. 6 (2023) 1055–1065.
[71] Y.-W. Lee, S. Chun, D. Son, X. Hu, M. Schneider, M. Sitti, A tissue adhesion-controllable and biocompatible small-scale hydrogel adhesive robot, Adv. Mater. 34 (13) (2022) 2109325.
[72] S. Roy, M. Halder, P. Ramprasad, S. Dasgupta, Y. Singh, D. Pal, Oxidized pullulan exhibits potent antibacterial activity against S. aureus by disrupting its membrane integrity, Int. J. Biol. Macromol. 249 (2023) 126049.
[73] X. Deng, D. Wang, D. Zhang, M. Sun, L. Zhou, Y. Wang, X. Kong, C. Yuan, Q. Zhou, Antibacterial quaternary ammonium chitosan/carboxymethyl starch/alginate sponges with enhanced hemostatic property for the prevention of dry socket, Front. Bioeng. Biotechnol. 10 (2023) 1083763.